AEDC-TR-69-1

EXPERIMENTAL INVESTIGATION OF TURBULENT STEP-INDUCED BOUNDARY-LAYER SEPARATION AT MACH NUMBERS 2.5, 3, AND 4

Jerry S. Hahn

ARO, Inc.

March 1969

VON KÁRMÁN GAS DYNAMICS FACILITY
ARNOLD ENGINEERING DEVELOPMENT CENTER
AIR FORCE SYSTEMS COMMAND
ARNOLD AIR FORCE STATION, TENNESSEE

NOTICES

When U. S. Government drawings specifications, or other data are used for any purpose other than a definitely related Government procurement operation, the Government thereby incurs no responsibility nor any obligation whatsoever, and the fact that the Government may have formulated, furnished, or in any way supplied the said drawings, specifications, or other data, is not to be regarded by implication or otherwise, or in any manner licensing the holder or any other person or corporation, or conveying any rights or permission to manufacture, use, or sell any patented invention that may in any way be related thereto.

Qualified users may obtain copies of this report from the Defense Documentation Center.

References to named commercial products in this report are not to be considered in any sense as an endorsement of the product by the United States Air Force or the Government.

EXPERIMENTAL INVESTIGATION OF TURBULENT STEP-INDUCED BOUNDARY-LAYER SEPARATION AT MACH NUMBERS 2.5, 3, AND 4

Jerry S. Hahn
ARO, Inc.

FOREWORD

The work reported herein was done at the request of Headquarters, Arnold Engineering Development Center (AEDC), Air Force Systems Command (AFSC), under Program Element 62201F, Project 8953, Task 03.

The results of tests presented were obtained by ARO, Inc. (a subsidiary of Sverdrup & Parcel and Associates, Inc.), contract operator of AEDC, AFSC, Arnold Air Force Station, Tennessee, under Contract F40600-69-C-0001. The tests were conducted intermittently within the period from April 29 to September 25, 1968, under ARO Project No. VD0883. The manuscript was submitted for publication on November 25, 1968.

The author wishes to acknowledge Dr. Jain-Ming Wu, Associate Professor of Aerospace Engineering, University of Tennessee Space Institute, and Captain Robert E. Wilson of the VKF for their suggestions which benefitted the author.

The author has also benefitted from the assistance of William T. Strike and J. Don Gray of the VKF Aerodynamics Section.

This technical report has been reviewed and is approved.

Eugene C. Fletcher
Lt Colonel, USAF
AF Representative, VKF
Directorate of Test

Roy R. Croy, Jr.
Colonel, USAF
Director of Test

ABSTRACT

An experimental investigation of turbulent separated boundary-layer flow was conducted using high ($3 \lesssim h/\delta \lesssim 13$) forward-facing steps (with side plates) mounted on a flat plate at zero angle of attack. The tests were made at Mach numbers of 2.5, 3.0, and 4.0 for Reynolds numbers, based on the boundary-layer total thickness at the separation location, from 0.10×10^6 to 0.15×10^6. The effects of Mach number, step height and span, end plates, and step-face fairings were investigated. Data are presented graphically and in tabulations and include model surface pressures on the flat plate and on the face and top of selected steps, boundary-layer Mach number profiles, and selected oil dot photographs.

CONTENTS

ILLUSTRATIONS

APPENDIX

Tables

NOMENCLATURE

EP	End plates (see Fig. 2)
h	Step height, in.
M	Local Mach number in boundary layer
M_δ	Mach number at outer edge of boundary layer
M_∞	Free-stream Mach number
p	Surface pressure, psia
p_∞	Free-stream static pressure, psia
Re_δ	Reynolds number based on boundary-layer total thickness at separation location
Re_∞	Free-stream unit Reynolds number, $in.^{-1}$
S	Step span, in.
x	Longitudinal distance downstream from the leading edge of flat plate, in.
y	Distance above and perpendicular to flat plate surface, in.
z	Lateral distance from model centerline (positive to the right, looking upstream), in.
δ	Boundary-layer total thickness (where $M \approx M_\delta$) (see Fig. 9)

SUBSCRIPTS

EP	Beginning of end plates
G	Beginning of carborundum grit roughness
s	Beginning of separation
step	Beginning of 90-deg step face

SECTION I
INTRODUCTION

The separation of a turbulent boundary layer induced by a forward-facing step has many practical applications and has been studied extensively. However, with the exception of Ref. 1, the investigations have usually been limited to relatively low* steps (e.g., Ref. 2).

The present tests are an extension of Wilson's work (Ref. 1) on very high forward-facing steps and were also made to check the two-dimensionality of his data which were obtained without end plates. In the present investigation, an attempt was made to fix the separation location at approximately 7.6 in. from the leading edge of the flat plate for all step heights by varying the step location on the plate. Three different sets of end plates, the beginnings of which were normally located at $x = 7.6$ in., were used in an attempt to obtain two-dimensional separation data and to study end plate effects. Inasmuch as pressure information on a step is scarce, pressure data on the face and top of several steps were obtained in addition to the pressure data in the separation zone on the flat plate. The tests were primarily conducted at $M_\infty = 3.0$; however, pressure data on the flat plate and step were obtained with one step height at $M_\infty = 2.5$ and 4.0. A pitot probe was employed to survey the boundary layer at two stations for all three Mach numbers.

SECTION II
APPARATUS

2.1 WIND TUNNEL

Tunnel D is an intermittent, variable density wind tunnel with a manually adjusted, flexible-plate-type nozzle and a 12- by 12-in. test section. The tunnel operates at Mach numbers from 1.5 to 5 at stagnation temperatures up to about 540°R. A more complete description of the tunnel and airflow calibration information may be found in Ref. 3.

---

*Low step as referred to here means that the step height is approximately equal to the boundary-layer thickness at the separation point.

2.2 MODEL

The model consisted of a 12-in. wide by 22-in. long flat plate, three pairs of triangular-shaped end plates, and seven steps of various widths and heights. With the exception of the end plates and the instrumented step, this is the model which was used in Ref. 1.

The plate was strut mounted as shown in Fig. 1a and had a rubber O-ring insert between the model and the tunnel wall to prevent the bleed of flow from one side of the plate to the other. The leading edge thickness was 0.004 ± 0.001 in., and the surface angle of inclination was less than 0.05 deg with respect to the tunnel centerline. The plate was installed about 1.5 in. below the tunnel centerline to prevent flow blockage when testing the larger steps.

Three different step heights and two different step spans provided a wide range of configurations for study (Fig. 1b). The three basic step heights were 0.485, 0.960, and 1.489 in., and by using various combinations of the steps, it was possible to vary the total step height between 0.485 and 1.920 in. The step spans were 3 and 6 in., and they could be mounted either individually or side by side to give spans up to 9 in. In order to maintain similar boundary-layer conditions at the separation location for all step heights, several sets of mounting holes were provided on the flat plate so that the steps could be moved longitudinally.

In an attempt to keep the separated flow field two-dimensional, two sets of triangular-shaped end plates with sweep angles of 31 and 20 deg were employed (Fig. 2). These sweep angles were selected from schlieren photographs (Fig. 3) of the model without end plates which showed that the separation shock wave angle and the angle of the separated viscous flow were approximately 31 and 20 deg, respectively, for all step heights where boundary-layer transition was upstream of separation. Later, a third set of end plates with a sweep angle of 31 deg, but of greater length, was fabricated in order to study the effects of longitudinal movement of the end plates on the pressure distribution in the separated region. The top portion of this set of end plates was removed so that the upper portion of the separation shock wave could be observed in high speed schlieren motion pictures. The most upstream point of this set of end plates could be placed in 1-in. increments from 3.6 to 7.6 in. from the leading edge of the flat plate, whereas the other two sets of end plates were fixed at $x = 7.6$ in.

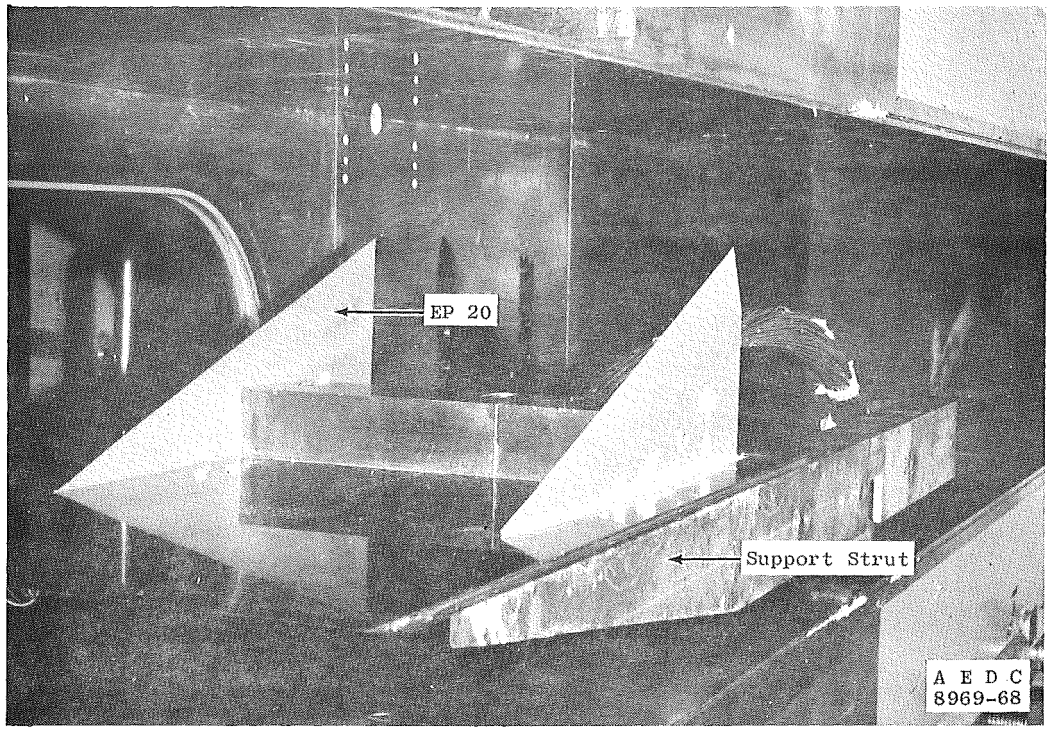

a. Model Installation

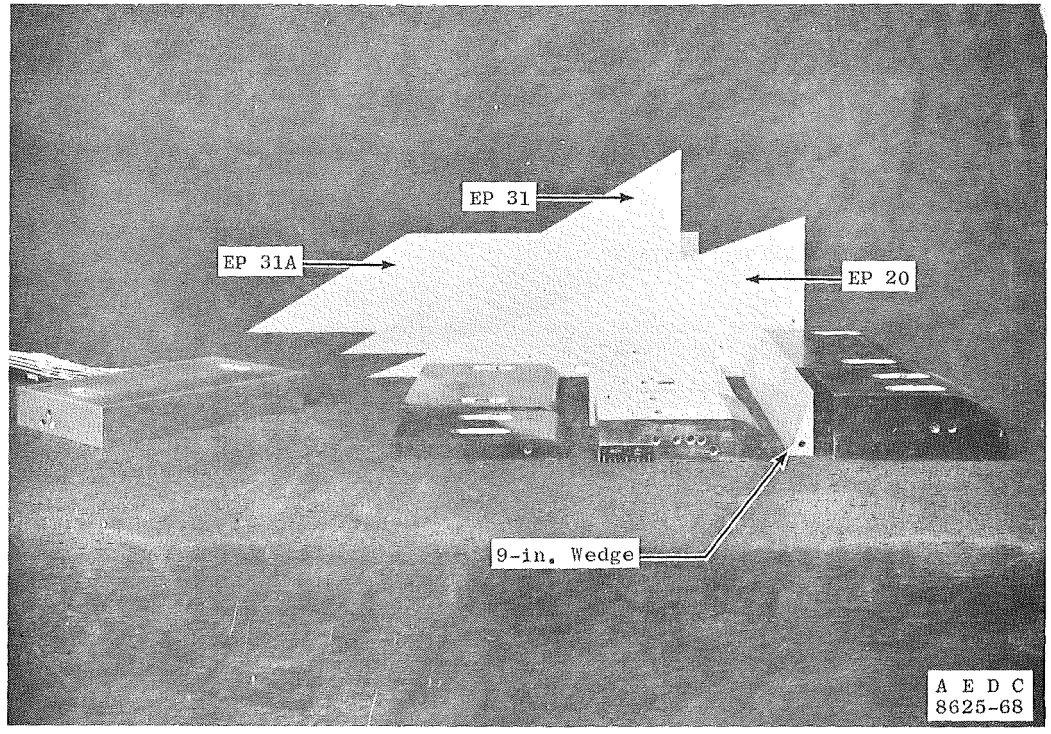

b. Steps, End Plates, and Wedge

Fig. 1 Photographs of Model Components

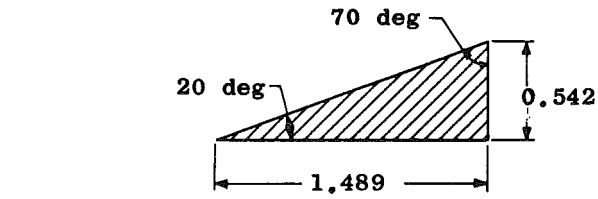

Cross Section of the 9-in. Wedge

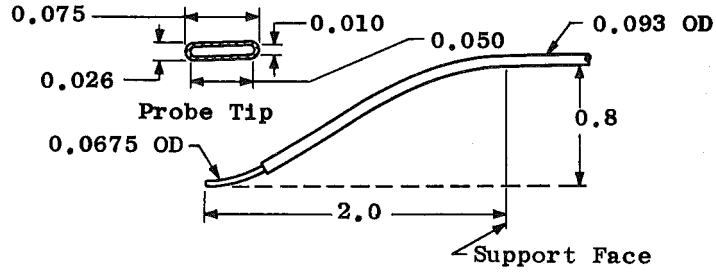

Pitot Probe

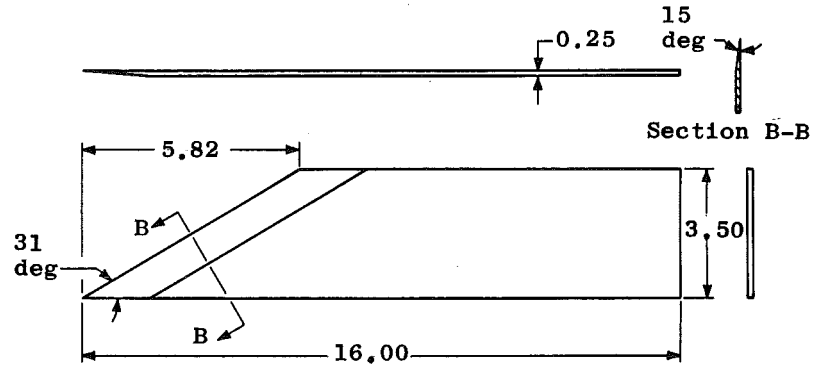

End Plate 31A

All Dimensions in Inches

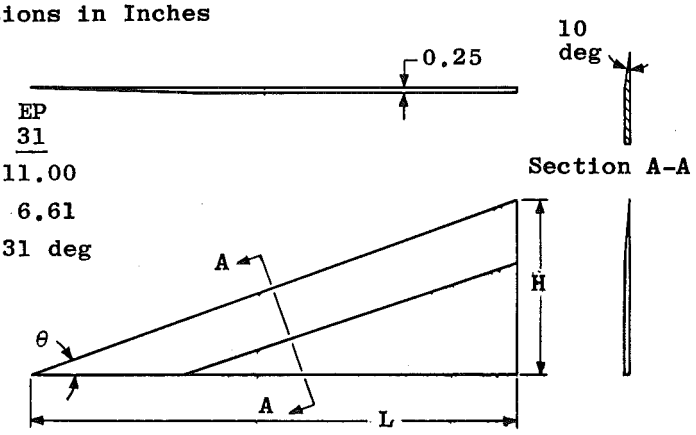

	EP 20	EP 31
L	13.00	11.00
H	4.73	6.61
θ	20 deg	31 deg

End Plate 20 or 31

Note: Only one of each of the three pairs of end plates is shown. The counterpart for each one is equal and opposite.

Fig. 2 Details of Model Components and Pitot Pressure Probe

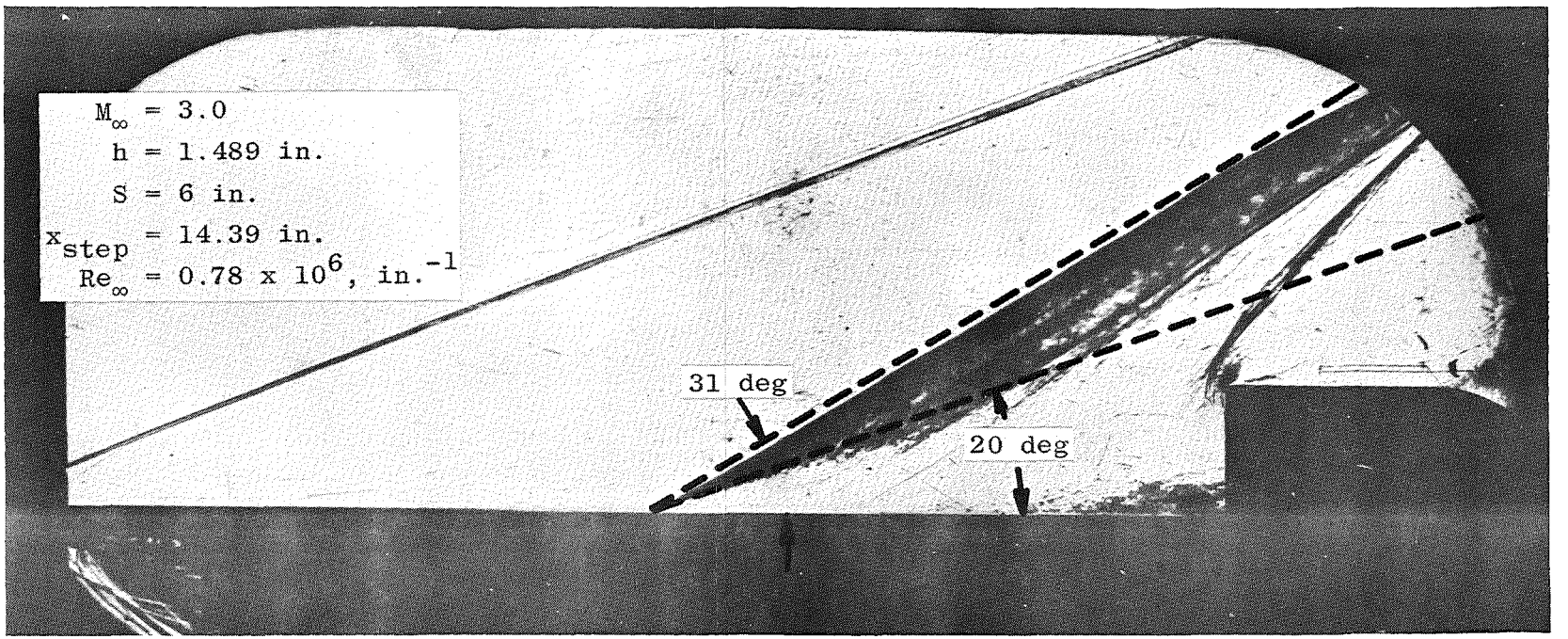

Fig. 3 Schlieren Photograph of the Model without End Plates

A 9-in. -span wedge, which attached to the end plates, was used with a 1.489-in. step to investigate the effects of step-face fairings upon the flat plate pressure distribution. A cross section of this wedge is given in Fig. 2, and the two different wedge positions tested are shown in a later figure.

All possible bleed passages were sealed with either vacuum grease or a sealant. Sealant was also employed on the hidden surfaces when the wedge was used.

A 0.25-in. -wide strip of Carborundum® grit roughness spanning the flat plate was used for selected conditions at $M_\infty = 3$ and at $M_\infty = 4$ to promote a turbulent boundary layer ahead of the separation location. See Table I (Appendix) for grit sizes and locations.

2.3 BOUNDARY-LAYER PROBE

A pitot pressure probe was employed to survey the boundary layer at two axial centerline stations in the absence of the end plates and steps. The probe drive mechanism was attached to a strut supported from an insert plate on the top wall of the tunnel (Fig. 4). The height of the probe tip centerline above the flat plate could be varied from 0.013 to 1.150 in. with an accuracy of ±0.004 in. Probe height was determined by a calibrated counter that was connected to the probe drive shaft. The probe tip was approximately elliptical as shown in Fig. 2.

2.4 INSTRUMENTATION AND TECHNIQUE

The flat plate portion of the model was instrumented to measure 59 pressures which were of interest in this investigation. This instrumentation included 29 centerline orifices that were equally spaced in 0.25-in. intervals beginning 7 in. downstream of the leading edge, and 14 orifices located in the vicinity of the separation location, either ±0.25 or ±0.50 in. off centerline. Also, a total of 16 spanwise orifices were distributed among three rows; the first row was located 8 in. from the leading edge and 3-in. intervals were left between succeeding rows.

One 0.960-in. step with a 6-in. span was instrumented to measure 18 pressures on the face and 14 on the top. This step could be stacked above or below other steps, permitting complete face-pressure distributions to be obtained for step heights greater than 0.960 in. When used side by side with the uninstrumented 0.960-in. step, the three vertical rows on the step face were located 0.25, 0.50, and 0.75 in. off model centerline and the longitudinal row on top of the step was 2 in. off centerline.

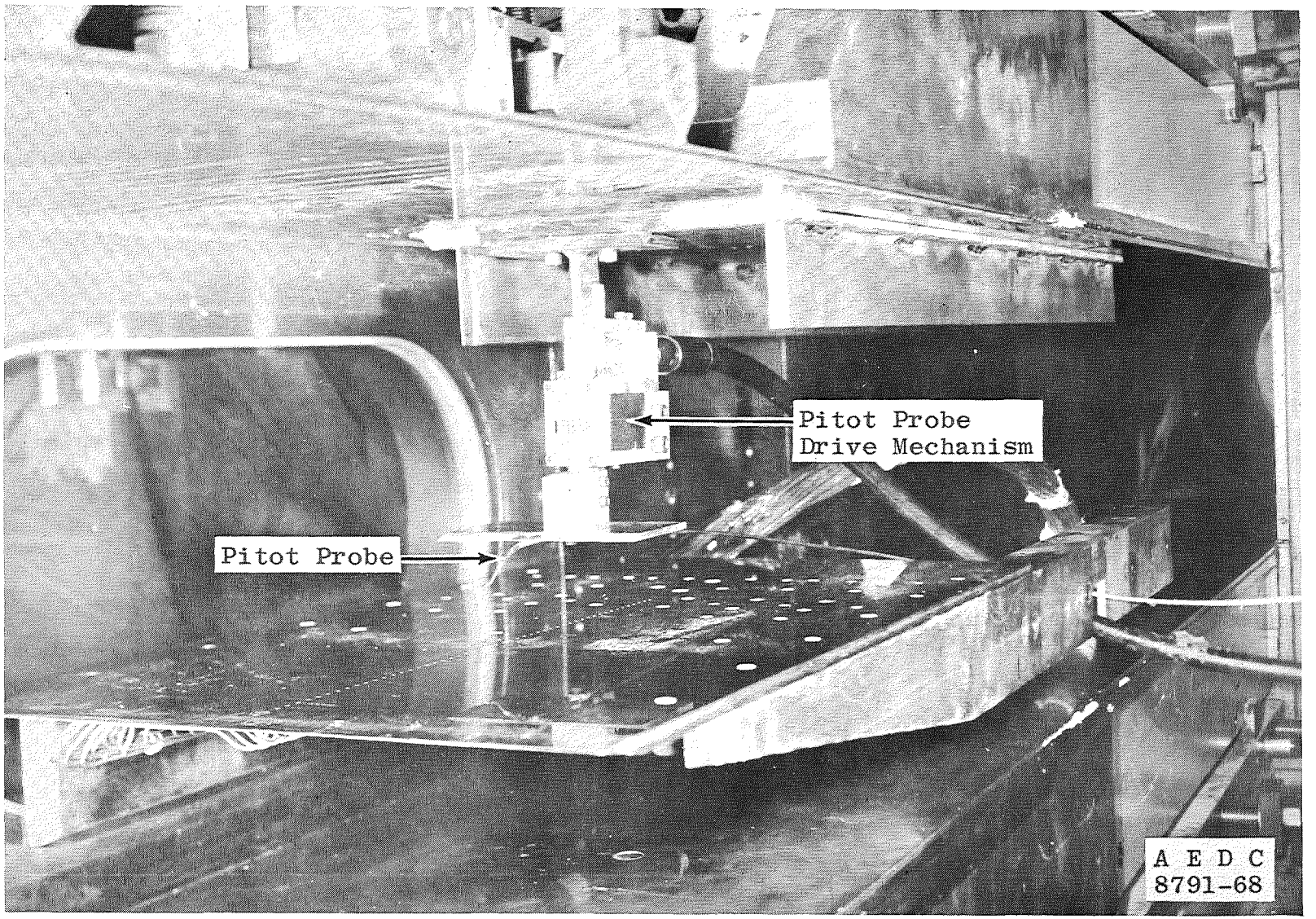

Fig. 4 Photograph of Pitot Pressure Probe Installation

All of the pressure orifice diameters were 0.040 in. Tables II, III, and IV give specific locations of the pressure orifices on the flat plate and the step. All the model surface pressures were measured with 15-psid transducers referenced to a near vacuum. These transducers have calibrated full-scale ranges of 1, 5, and 15 psia and are considered accurate to within ±0.3 percent of full scale for each range.

In order to determine the flow separation location, either oil flow or oil dot techniques were used. Zyglo® penetrating oil was sprayed on the model to obtain oil flow photographs, and a relatively viscous mixture of titanium dioxide and vacuum pump oil was used to make the oil dots. Typical results from the oil dot technique are shown later. Values of the separation location at the model centerline are presented in Table I, which is a summary of the model configurations and corresponding test conditions.

Inasmuch as Bogdonoff (Ref. 2) and others have observed unsteady motions of the shock system, high speed schlieren motion pictures of the separation and reattachment shock waves were taken during most runs. These data have not been analyzed; however, unsteady motions in the flow were observed. Although spark schlieren (0.25-μsec duration) photographs were also taken during each run, no photographs corresponding to the data are presented since the end plates obscured most of the flow region of interest.

SECTION III
RESULTS AND DISCUSSION

3.1 FLAT PLATE DATA

The greatest influence of end plates was observed with the narrowest step span (S = 3.0 in.). Static pressure distributions for a 1.489-in. step of this span are presented in Fig. 5a. As would be expected, the start of the pressure rise was delayed and the plateau pressure was lower without end plates because of the spanwise outflow from the high pressure separated region. The larger end plates (EP 31), which enclosed the entire separated flow field (Fig. 3), forced separation to occur earlier with this span (S = 3.0 in.) than did the smaller end plates (EP 20), which enclosed approximately just the viscous portion of the separated flow. However, downstream of the plateau, the pressure distributions for the two basic

sets of end plates were identical. It is important to note that the distributions for the two sets of end plates are also nearly identical upstream of the plateau if the distributions are moved longitudinally so that the flow separation location is matched.

In Fig. 5b, pressure distributions ahead of the 1.489-in. step with large end plates (EP 31) are presented for the two extreme spans which were tested. As shown, model span had no effect on the centerline pressure distribution in the recirculating flow region; however, pressure data without end plates (Ref. 1) were significantly affected by a span change. In addition, it is shown in Fig. 5c that there was no significant effect of a 4-in. axial movement of the end plates for a 0.960-in. step.

In order to study the effect of step-face fairings, a wedge which could be oriented in two different positions relative to the flow (20 or 70 deg) was mounted against the face of a 1.489-in. step. It is shown in Fig. 5d that, with respect to a standard step, the beginning of the pressure rise occurred earlier with the 20-deg wedge configuration but later with the 70-deg wedge configuration. However, once the plateau was reached, the distributions were nearly identical, except very close to the wedge. Once again, the three pressure distributions are nearly identical upstream of the plateau when observed with the beginning of separation as a common origin.

Pressure data at all three test Mach numbers are presented in Fig. 5e for a 0.960-in. step with a span of 9 in. and end plates (EP 31A). The boundary layer was naturally turbulent prior to separation at M_∞ = 2.5 and 3.0, but a trip of Carborundum grit roughness was required at M_∞ = 4.0 to promote a turbulent separation. The three distributions are similar with Mach number having almost no effect on the location of the beginning of the pressure rise.

In Fig. 6, typical spanwise pressure distributions on the flat plate at two stations (x = 8 and 11 in.) are presented for various step configurations. The distributions were fairly uniform for all step heights with the data for the 0.960-in. step being the least uniform at both stations. Pressure data at x = 11 in. were more nearly uniform than that at x = 8 in. since the latter were obtained in a region of very high pressure gradient and, thus, any slight spanwise variation of the separation point would be expected to affect the uniformity significantly.

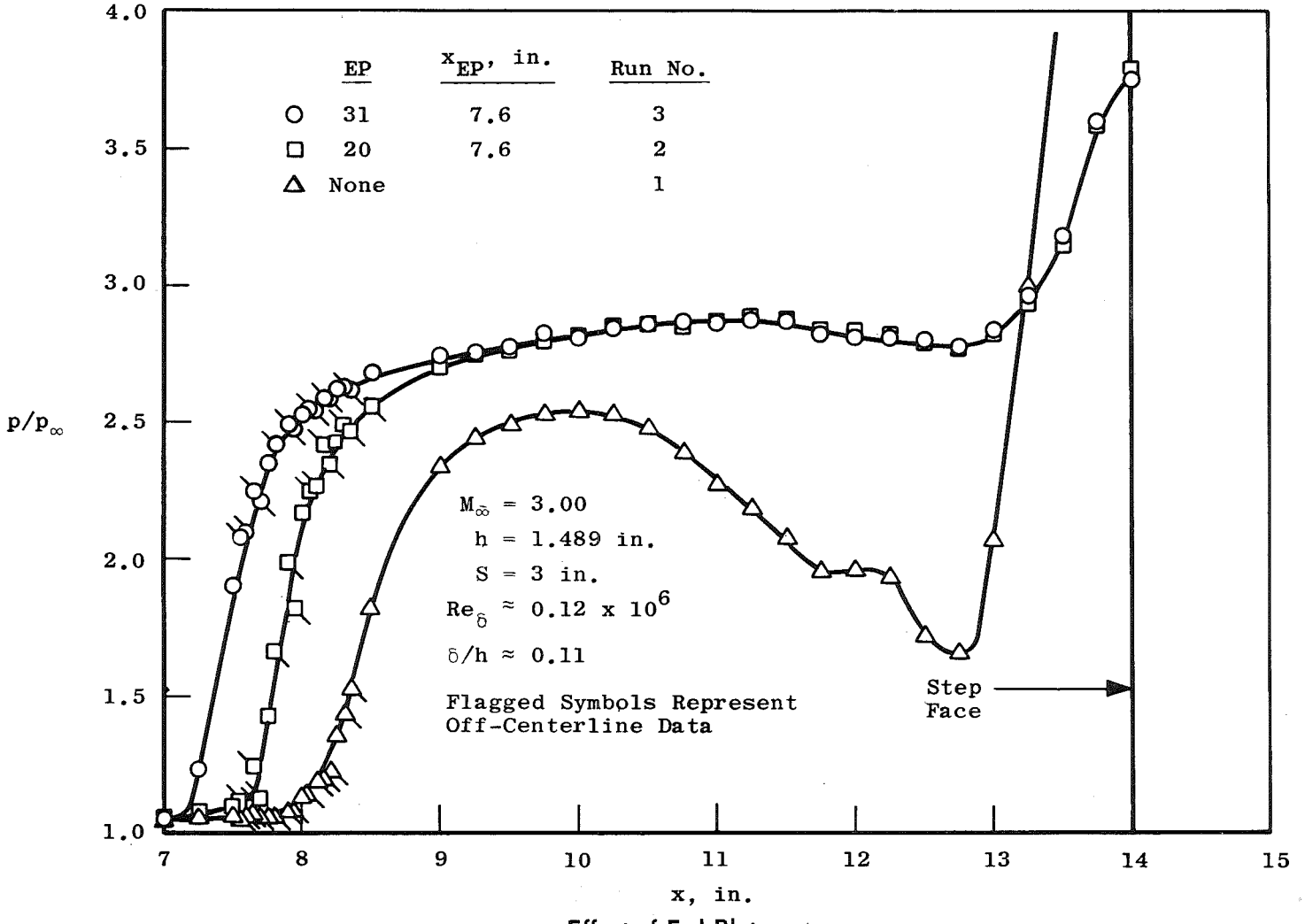

a. Effect of End Plates

Fig. 5 Centerline Pressure Distributions on the Flat Plate

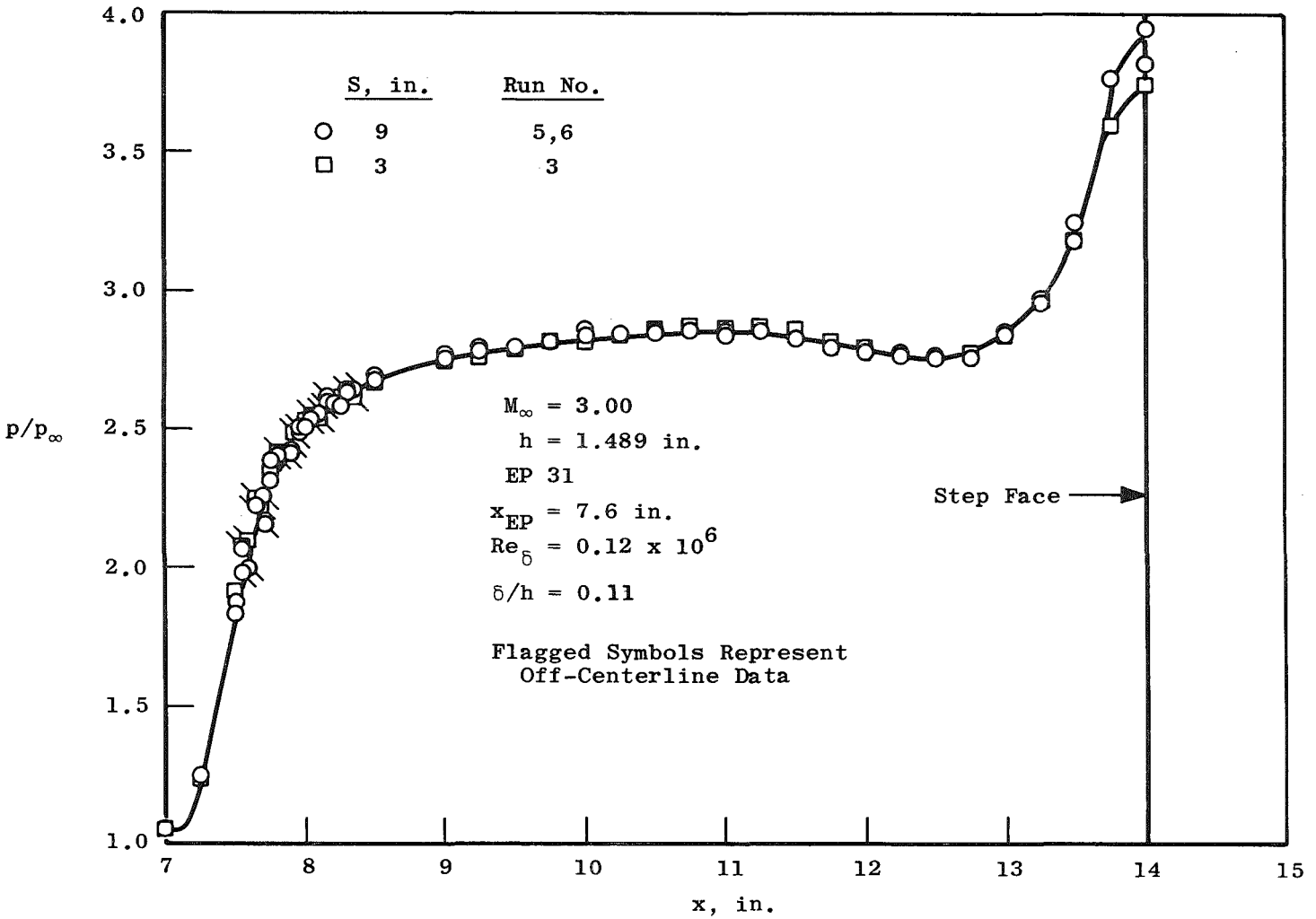

b. Effect of Step Span for Model with End Plates

Fig. 5 Continued

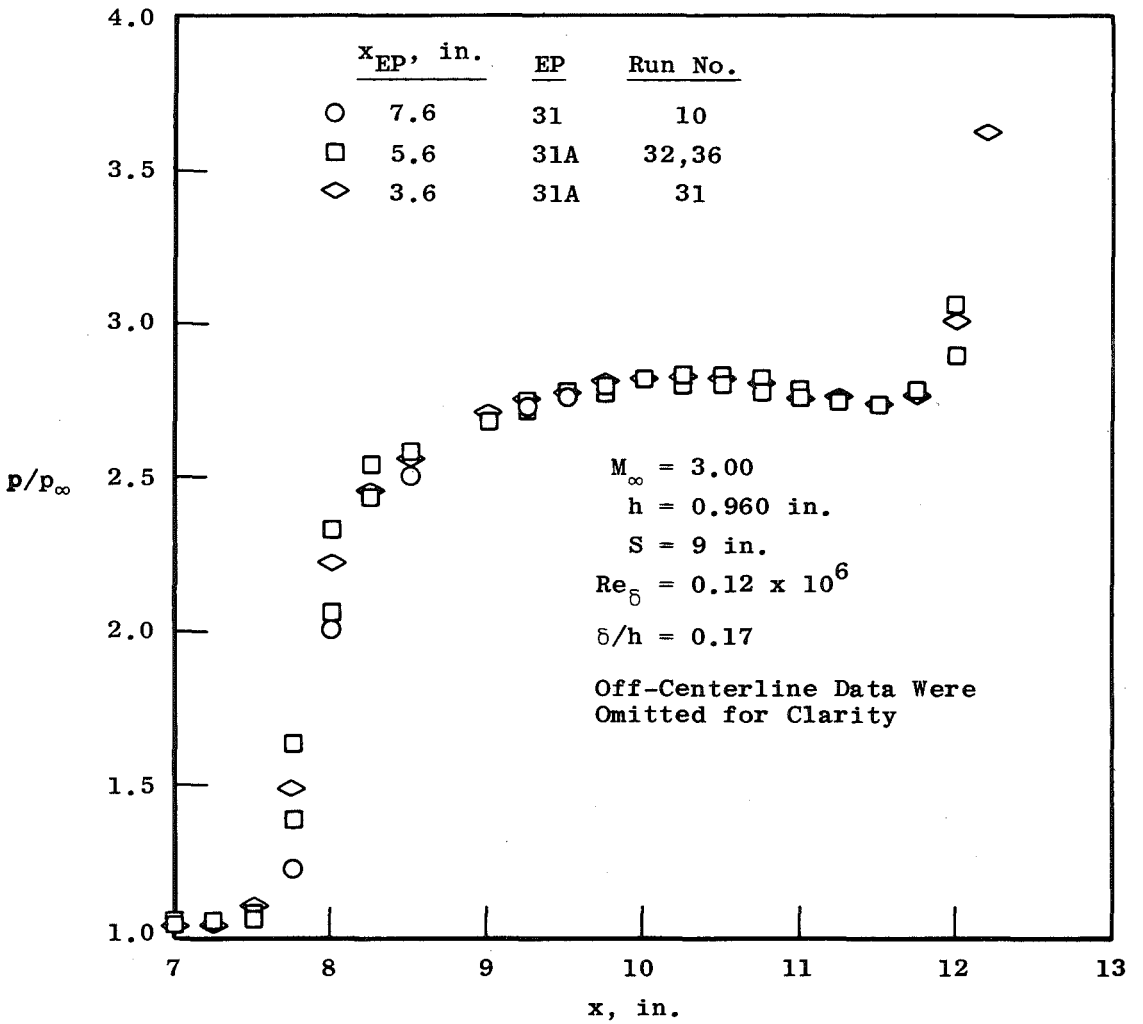

c. Effect of Longitudinal Movement of End Plates

Fig. 5 Continued

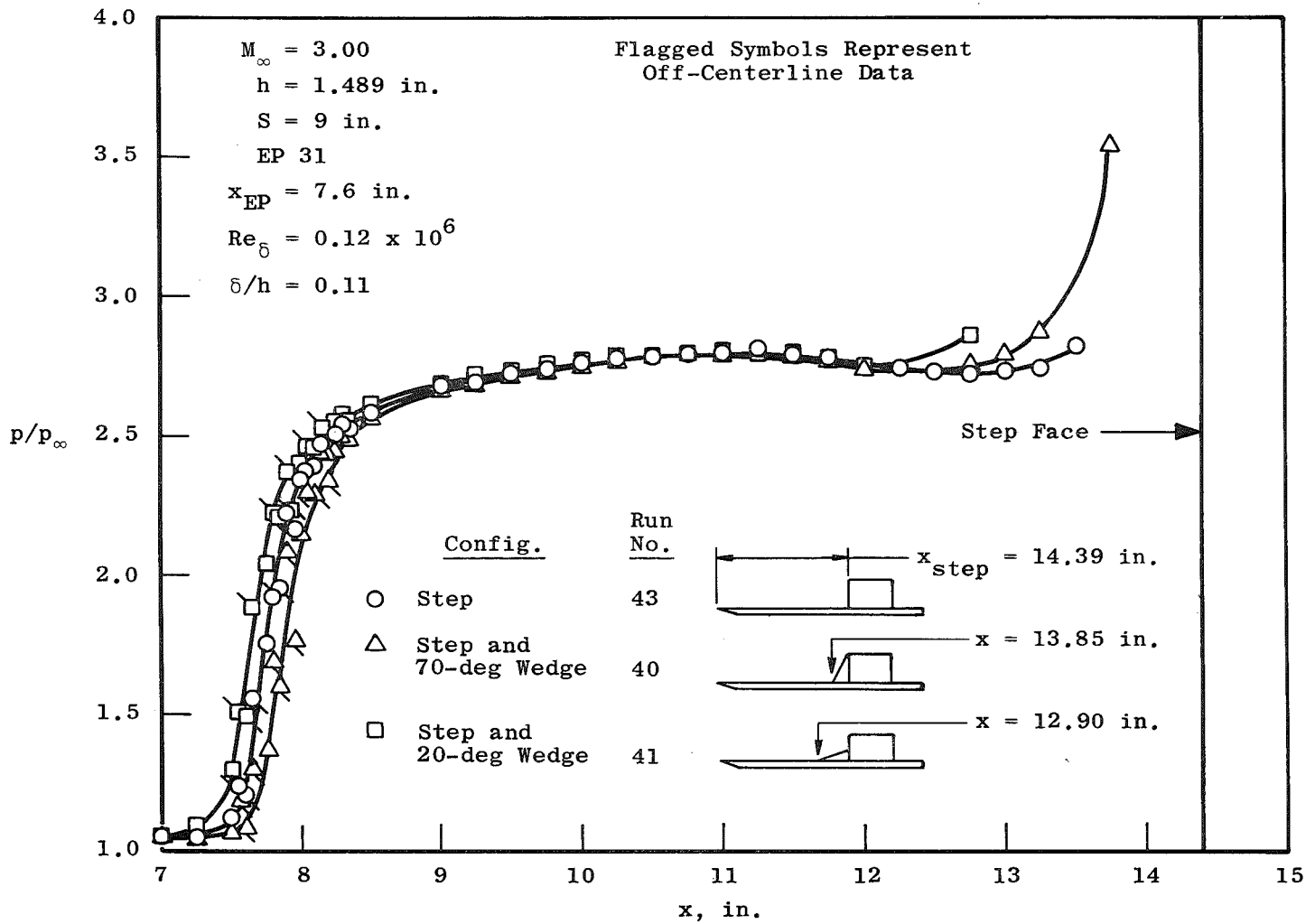

d. Effect of Step-Face Fairing

Fig. 5 Continued

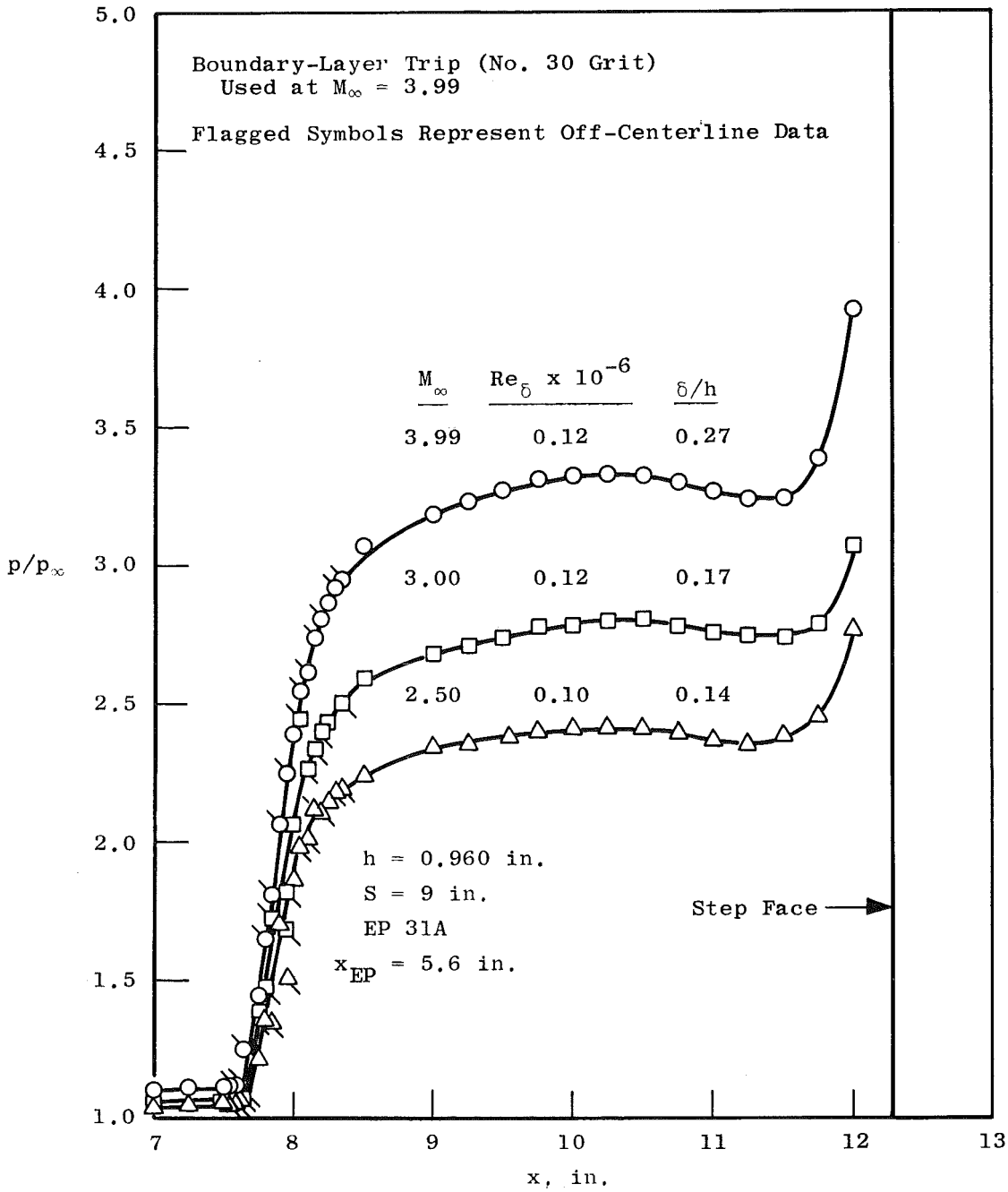

e. Effect of Mach Number

Fig. 5 Concluded

	h, in.	δ/h	EP	x_{EP}, in.	Run No.
○	1.489	0.11	31	7.6	5,6
□	0.985	0.16	31	7.6	7,8
◇	0.960	0.17	31A	5.6	34,36
△	0.485	0.33	31	7.6	9

$M_\infty = 3.00$
$S = 9$ in.
$Re_\delta = 0.12 \times 10^6$

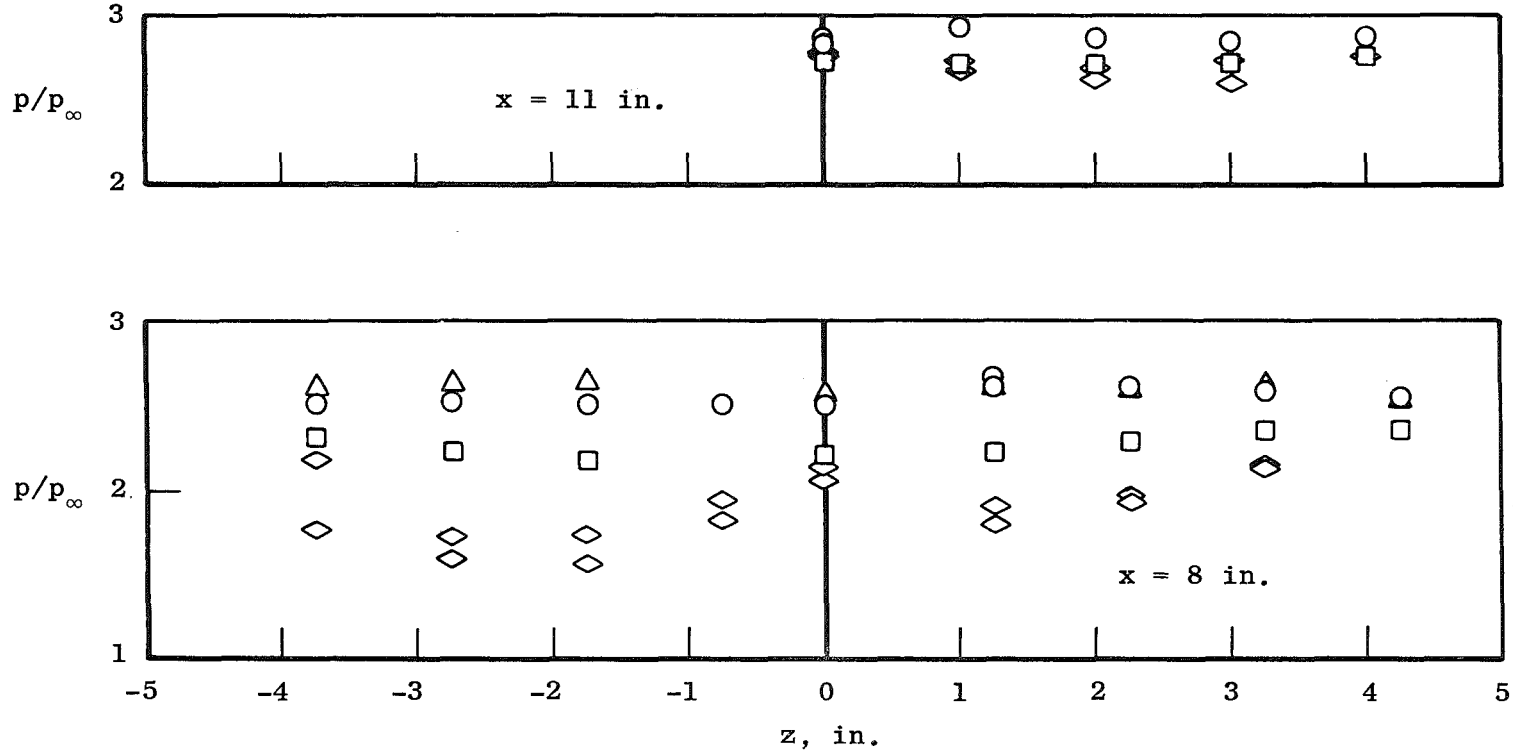

Fig. 6 Spanwise Pressure Distributions on the Flat Plate

Oil dot photographs which show the effect of end plates on the separation induced by a 1.489-in. step with a span of 9 in. are presented in Fig. 7. For this step without end plates, the lateral outflow from the recirculating region can readily be established by observing the flow direction of the oil dots and the continuous curvature of the separation line. As noted previously, the separation location at model centerline was nearer the step without end plates because of the three-dimensionality of the flow. The separation line was nearly straight when the largest end plates (EP 31) were used. However, when the smaller end plates (EP 20) were used, the separation line was somewhat curved on one side. This asymmetry was possibly created by a small asymmetrical streamwise alignment of the end plates. Nevertheless, the separation location at model centerline was the same for the two basic sets of end plates. This does not contradict the data shown in Fig. 5a since differences in the separation location for the two basic sets of end plates were smaller as the step span was increased. Hence, it is considered that the flow near the model centerline was typically two-dimensional with the end plates. Tabulations of the flat plate pressure data are given in Table II.

3.2 STEP DATA

Inasmuch as information concerning pressures on the face and top of steps is scarce, such pressure data for several steps with end plates were obtained, and tabulated results are given in Tables III and IV. The scatter in these data is quite large and is attributed, at least in part, to unsteady motions of the shock system which were observed for steps both with and without end plates. In particular, significant changes with time in the flow field just upstream of reattachment were observed using high speed schlieren motion pictures.

Some typical step-face pressure distributions are presented in Fig. 8. The effects of end plates and step height and span can all be seen in Fig. 8a. Pressure distributions for the two basically different sets of end plates were nearly identical over the lower half of the step face; however, the pressure rise on the upper half was generally greater when the smaller end plates were used. Moreover, the effect of increasing the span (using the large end plates) was to increase the pressures near the top of the step face. (Note the different locations on the pressure orifices from centerline in Tables III and IV for these two spans.) Finally, the effect of step height (using the large end plates) on the step face pressure was more pronounced near the top of the step face. All three effects may be caused, in part, by the boundary-layer growth on the large end plates which captured more of the inviscid flow above the reverse flow region

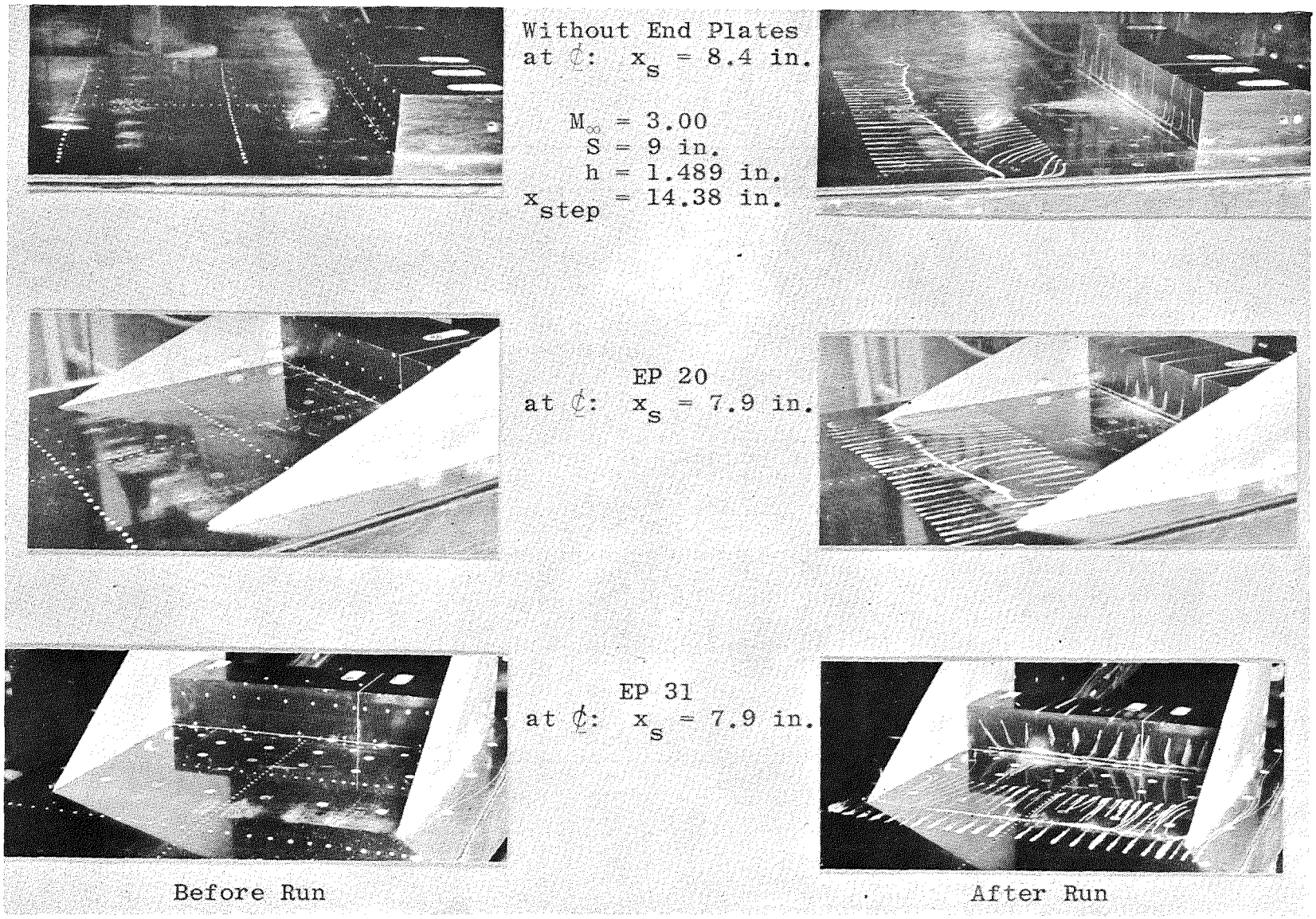

Fig. 7 Oil Dot Photographs

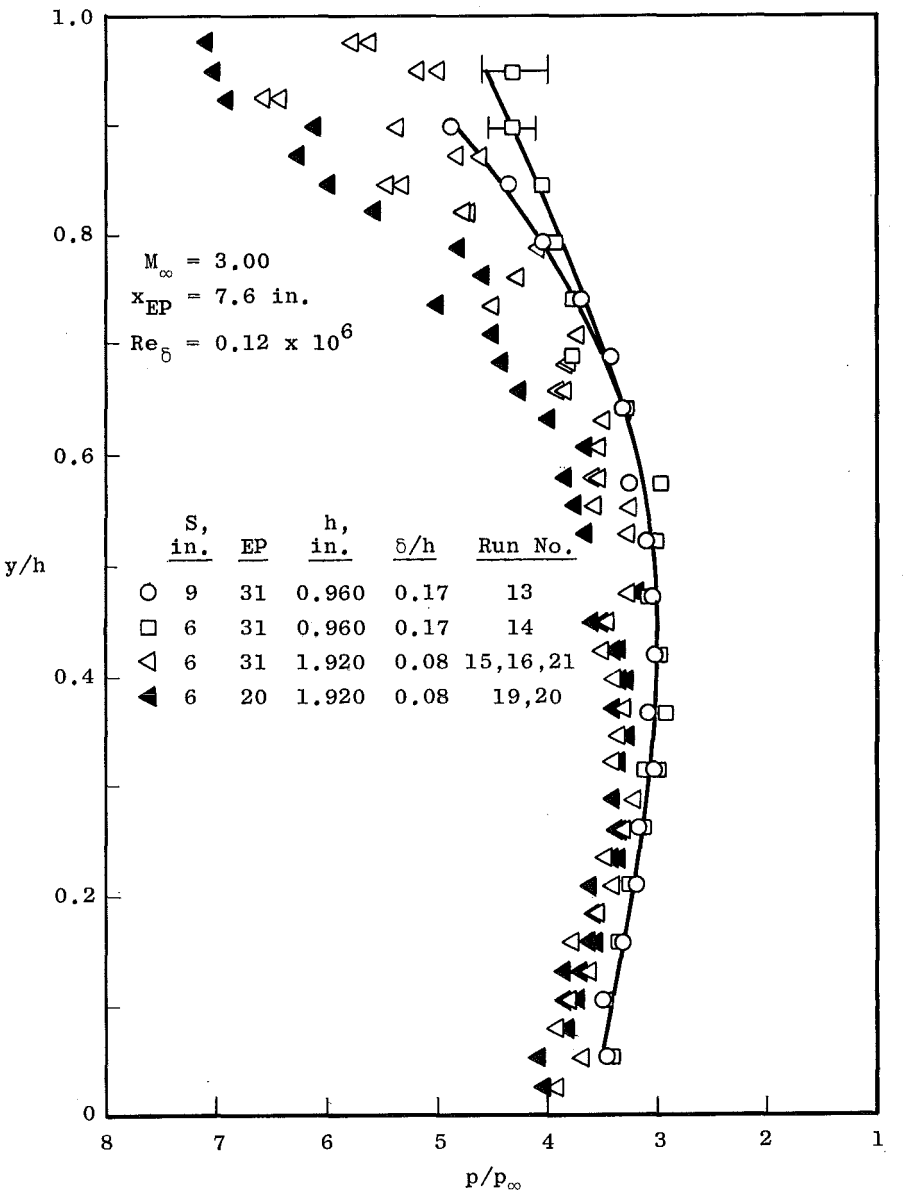

a. Effects of End Plates, Step Height, and Step Span

Fig. 8 Pressure Distributions on the Step Face

	M_∞	EP	x_{EP}, in.	$Re_\delta \times 10^{-6}$	δ/h	Run No.
○	3.99	31A	5.6	0.12	0.27	47
□	3.00	31A	5.6	0.12	0.17	45
■	3.00	31	7.6	0.12	0.17	13
⧄	3.00	31	7.6	0.12	0.17	10
◁	2.50	31A	5.6	0.10	0.14	46

h = 0.960 in.

S = 9 in.

Boundary-Layer Trip (No. 30 Grit)
Used at M_∞ = 3.99

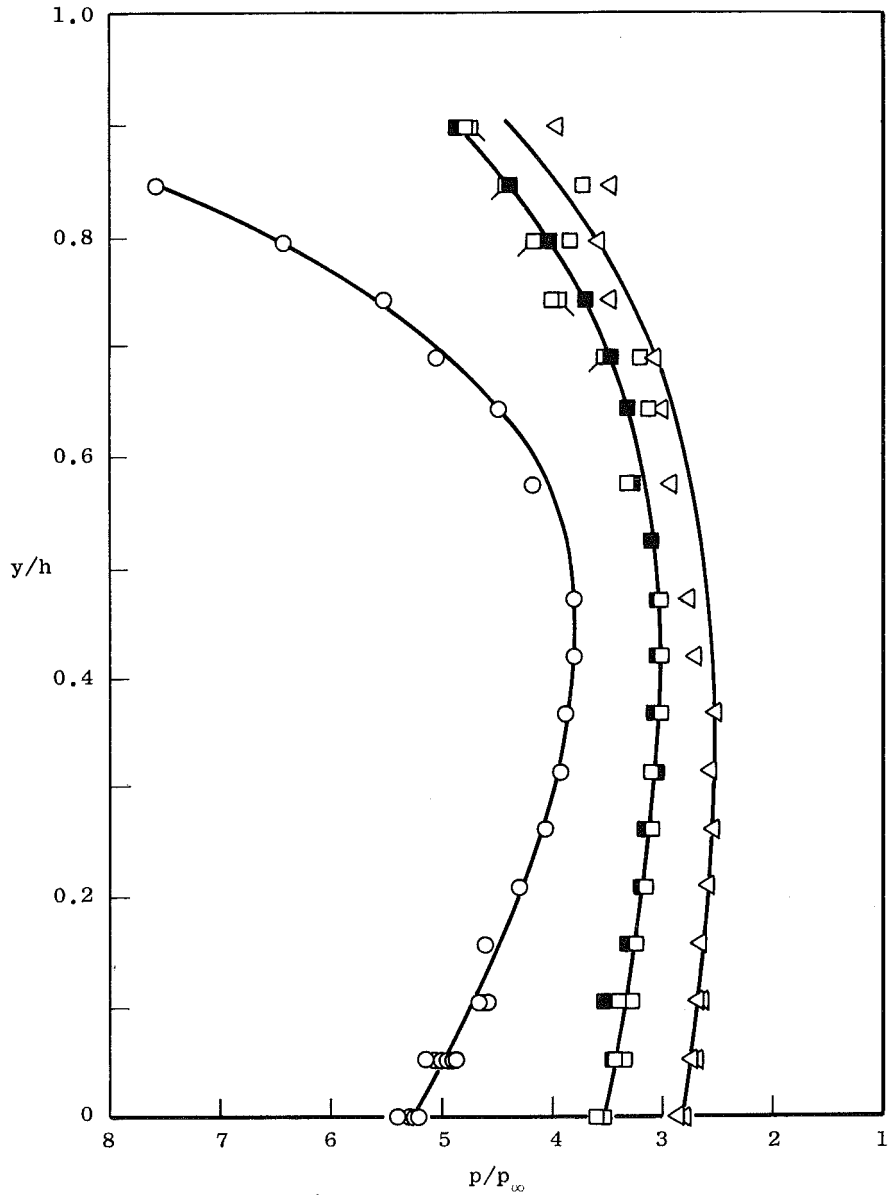

b. Effect of Mach Number

Fig. 8 Concluded

than did the smaller end plates. These results show that the reattachment region was the most sensitive region to changes in model geometry and, hence, to small deviations from two-dimensional flow.

Pressure distributions on the face of a 0.960-in. step with a 9-in. span are presented in Fig. 8b for the three test Mach numbers. Because of the increase in the plateau pressure with Mach number, there was a significant increase in the pressure level on the step face. The incremental increase in pressure level across the step face was approximately constant for a Mach number increase from 2.5 to 3.0. However, the pressure data at $M_\infty = 4.0$ showed a more rapid pressure rise near the bottom and top of the step face. Even with these high pressure gradients, the data at $M_\infty = 4.0$ had less scatter than the data at $M_\infty = 2.5$ and 3.0.

3.3 PITOT PROBE DATA

In Fig. 9, the Mach number profiles obtained with the pitot pressure probe are presented for $M_\infty = 2.5$, 3.0, and 4.0 at model stations 7.6 and 14.1 in. from the leading edge of the flat plate. The pitot survey data were obtained for $Re_\infty/in. = 0.78 \times 10^6$ at $M_\infty = 2.5$ and 3.0 and for $Re_\infty/in. = 0.48 \times 10^6$ at $M_\infty = 4.0$. These results indicate that the boundary-layer profiles were characteristically turbulent in all cases, although turbulent growth rates were not obtained in all cases, particularly for the higher Mach number data with roughness.

REFERENCES

1. Wilson, Robert E. "An Experimental Investigation of Separated Turbulent Supersonic Flow at $M_\infty = 3.0$." Masters Thesis, University of Tennessee, June 1966.

2. Bogdonoff, S. M. "Some Experimental Studies of the Separation of Supersonic Turbulent Boundary Layers." Princeton University Report 336, June 1955.

3. Anderson, A. "Flow Characteristics of a 12-in. Intermittent Supersonic Tunnel." AEDC-TDR-63-203 (AD418578), September 1963.

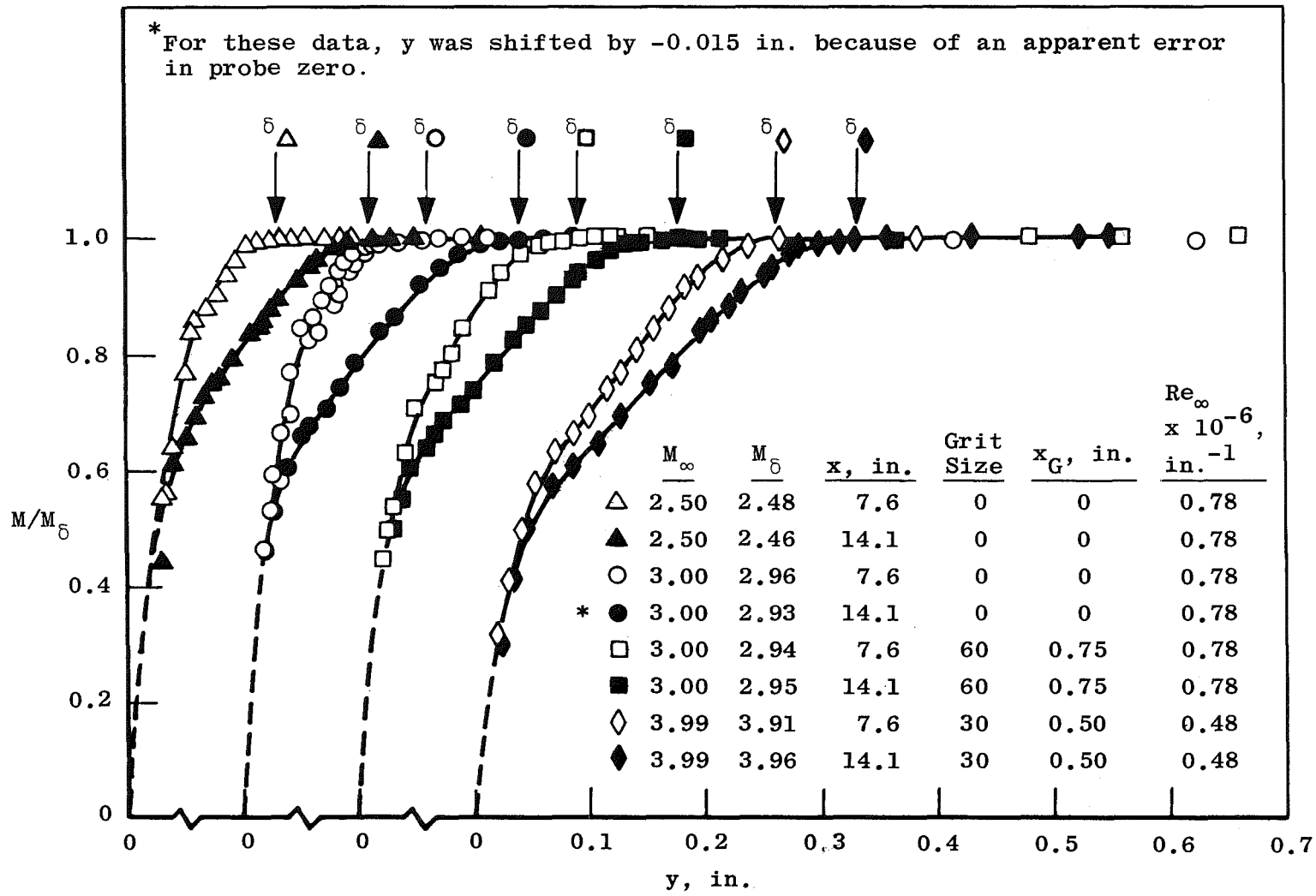

Fig. 9 Boundary-Layer Mach Number Profiles

APPENDIX
TABLES

TABLE I
TEST SUMMARY

Configuration	Run Number	h, in.	x_{step}, in.	S, in.	EP	x_{EP}, in.	Grit Size	x_G, in.	x_S, in.	M_∞	Stilling Chamber Conditions		$Re_\infty \times 10^{-6}$, in.$^{-1}$	Pressure Data		
											Pressure, psia	Temperature, °R		Flat Plate	Step Face	Top of Step
Step	9	0.485	9.69	9	31	7.6	0		7.5	3.00	60	538	0.78	X		
	45	0.960	12.06	9	31A	5.6	0		7.7	3.00	↓	↓	↓	X	X	X
	**46	↓	↓	↓	↓	↓	↓	↓	7.7	2.50	45	530	↓	X	X	X
	47	↓	↓	↓	↓	↓	30	0.50	7.8	3.99	60	532	0.48	X	X	X
	12	↓	12.23	6	31	7.6	0	↓	8.0	3.00	↓	538	0.78	X		X
	10	↓	↓	9	↓	↓	↓	↓	8.0	↓	↓	↓	↓	X	X	X
	11	↓	↓	↓	↓	↓	60	0.75	7.9	↓	↓	↓	↓	X	X	↓
	30	↓	12.28	↓	None	↓	0	↓	↓	↓	↓	↓	↓	X	↓	↓
	31	↓	↓	↓	31A	3.6	↓	↓	↓	↓	↓	↓	↓	X	↓	↓
	32,34,36	↓	↓	↓	↓	5.6	↓	↓	↓	↓	↓	↓	↓	X	↓	↓
	33	↓	↓	↓	↓	↓	60	0.75	↓	↓	↓	↓	↓	X	↓	↓
	37	↓	↓	↓	↓	↓	30	0.50	7.8	3.99	↓	532	0.48	X	↓	↓
	38	↓	↓	↓	↓	↓	0	↓	7.9	2.50	45	530	0.78	X	↓	↓
	14	↓	12.43	6	31	7.6	↓	↓	↓	3.00	60	538	↓	X	X	X
	13	↓	↓	9	↓	↓	↓	↓	↓	↓	↓	↓	↓	X	X	X
	7,8	*0.985	12.22	9	↓	↓	0	↓	↓	↓	↓	↓	↓	X	↓	↓
	4	↓	12.30	3	↓	↓	↓	↓	↓	↓	↓	↓	↓	X	↓	↓
	23	1.445	14.38	6	20	↓	0	↓	↓	↓	↓	↓	↓	X	X	X
	22,24	↓	↓	↓	31	↓	↓	↓	↓	↓	↓	↓	↓	X	X	X
	1	1.489	14.00	3	None	↓	0	↓	↓	↓	↓	↓	↓	X	↓	↓
	2	↓	↓	↓	20	7.6	↓	↓	↓	↓	↓	↓	↓	X	↓	↓
	3	↓	↓	↓	31	↓	↓	↓	↓	↓	↓	↓	↓	X	↓	↓
	5,6	↓	↓	9	↓	↓	↓	↓	↓	↓	↓	↓	↓	X	↓	↓
	29	↓	14.39	6	None	↓	↓	↓	↓	↓	↓	↓	↓	X	↓	↓
	28	↓	↓	↓	20	7.6	↓	↓	↓	↓	↓	↓	↓	X	↓	↓
	27	↓	↓	↓	31	↓	↓	↓	↓	↓	↓	↓	↓	X	↓	↓
	43	↓	↓	9	↓	↓	↓	↓	7.9	↓	↓	↓	↓	X	↓	↓
Step and 20-deg Wedge	40	↓	↓	↓	↓	↓	↓	↓	↓	↓	↓	↓	↓	X	↓	↓
Step and 70-deg Wedge	41	↓	↓	↓	↓	↓	↓	↓	7.8	↓	↓	↓	↓	X	↓	↓
	18	1.920	16.00	6	20	7.6	↓	↓	↓	↓	↓	↓	↓	X	↓	↓
	19,20	↓	↓	↓	↓	↓	↓	↓	↓	↓	↓	↓	↓	X	X	X
	17	↓	↓	↓	31	↓	↓	↓	↓	↓	↓	↓	↓	X	↓	↓
	15,16,21	↓	↓	↓	↓	↓	↓	↓	↓	↓	↓	↓	↓	X	X	X

*Step from Ref. 1 before Modification

**Data Suspected to be Transitional Near the Separation Point

TABLE II
TABULATED PRESSURE DATA FOR THE FLAT PLATE

x, in.	z, in.	Run Number								
		1	2	3	4	5, 6	7, 8	9	10	11
		Static Pressure Ratio, p/p_∞								
7.00	0	1.044	1.051	1.051	1.045	1.053	1.053	1.060		
7.25	↓	1.056	1.067	1.235	1.062	1.246	1.070	1.076		
7.50	↓	1.064	1.087	1.905	1.102	1.832, 1.883	1.075, 1.068	1.864		
7.55	0.25	1.048	1.110	2.081	1.167	1.979, 2.068	1.095, 1.083	2.087	1.098	1.103
7.60	-0.25	1.056	1.106	2.099	1.151	1.998	1.112	2.200	1.104	1.194
7.65	0.50	1.066	1.239	2.252	1.448	2.223	1.153	2.340		
7.70	-0.50	1.056	1.124	2.212	1.182	2.155, 2.259	1.191, 1.191	2.378		
7.75	0	1.056	1.418	2.351	1.794	2.314, 2.387	1.376, 1.359	2.401	1.244	
7.80	0.25	1.060	1.663	2.418	2.057	2.396	1.593	2.465	1.342	1.654
7.85	-0.25									1.799
7.90	0.50	1.080	1.990	2.493	2.290	2.508, 2.526	1.937, 1.903	2.564		
7.95	-0.50	1.082	1.819	2.474	2.122	2.485, 2.505	2.093, 2.067	2.598		
8.00	0	1.127	2.167	2.532	2.343	2.510	2.221	2.574	2.008	2.075
8.05	0.25	1.141	2.253	2.549	2.407	2.536	2.226			2.151
8.10	-0.25	1.185	2.267	2.545	2.363	2.546, 2.561	2.333, 2.337	2.621		2.156
8.15	0.50	1.201	2.422	2.591	2.516	2.596, 2.620	2.414, 2.401	2.670	2.326	
8.20	-0.50	1.225	2.353	2.589	2.406	2.591	2.465	2.700	2.333	
8.25	0	1.356	2.433	2.617	2.496	2.578	2.459, 2.456	2.663		2.291
8.30	0.25	1.436	2.492	2.630	2.545	2.630, 2.642	2.503, 2.486	2.702		2.333
8.35	-0.25	1.529	2.474	2.619	2.486	2.638, 2.646	2.522, 2.515	2.707	2.434	2.354
8.50	0	1.823	2.561	2.679	2.585	2.677, 2.690	2.578	2.748	2.511	2.425
9.00	↓	2.341	2.697	2.740	2.670	2.769, 2.756	2.701, 2.689	2.693		2.560
9.25	↓	2.442	2.738	2.754	2.699	2.783, 2.788	2.753, 2.743	2.692	2.732	
9.50	↓	2.495	2.769	2.782	2.736	2.800, 2.806	2.791, 2.773	2.945	2.766	
9.75	↓	2.529	2.803	2.826	2.749	2.822	2.807, 2.800			
10.00	↓	2.542	2.821	2.813	2.763	2.867, 2.842	2.840, 2.834			
10.25	↓	2.529	2.848	2.844	2.759	2.854, 2.858	2.832, 2.827			2.711
10.50	↓	2.481	2.858	2.861	2.752	2.847, 2.855	2.838, 2.816			2.701
10.75	↓	2.394	2.846	2.871	2.716	2.863	2.826			2.676
11.00	↓	2.280	2.873	2.866	2.694	2.855, 2.842	2.738, 2.735			2.648
11.25	↓	2.187	2.890	2.876	2.686	2.857, 2.858	2.742, 2.732			2.636
11.50	↓	2.077	2.879	2.868	2.740	2.829, 2.834	2.782, 2.764			2.653
11.75	↓	1.958	2.839	2.825	2.796	2.797	2.882			2.713
12.00	↓	1.963	2.837	2.814	3.146	2.778, 2.805	3.345, 3.339			3.046
12.25	↓	1.931	2.815	2.808		2.768, 2.782				
12.50	↓	1.721	2.793	2.798		2.757, 2.769				
12.75	↓	1.655	2.767	2.775		2.758				
13.00	↓	2.072	2.821	2.838		2.854, 2.841				
13.25	↓	3.003	2.927	2.965		2.982, 2.956				
13.50	↓	4.538	3.141	3.180		3.253, 3.177				
13.75	↓	6.280	3.584	3.597		3.769				
14.00	↓	5.768	3.789	3.750		3.947, 3.818				
8.00	-3.75					2.521	2.322	2.609		
↓	-2.75					2.529	2.241	2.637		
↓	-1.75					2.510	2.175	2.651	1.771	
↓	-0.75				2.043	2.517				
↓	1.25	1.101	2.197	2.503	2.411	2.682, 2.610	2.212, 2.230	2.622	2.091	
↓	2.25					2.615	2.297	2.606	2.091	
↓	3.25					2.590	2.364	2.602		
↓	4.25					2.548	2.373	2.543	2.285	
11.00	1.00	2.247	2.927	3.034	2.868	2.943	2.751, 2.738		2.778	
↓	2.00					2.872	2.726			
↓	3.00					2.857	2.723			
↓	4.00					2.877	2.773			
14.00	1.00	5.102	3.351	3.381		3.740				
↓	2.00					3.595				
↓	3.00					3.678				
↓	4.00					3.631				

TABLE II (Continued)

x, in.	z, in.	Run Number							
		12	13	14	15-17, 21	18-20	22	23	24
		Static Pressure Ratio, p/p_∞							
7.00	0				1.108	1.042			
7.25	↓				1.275	1.054			
7.50				1.075	1.835 to 1.954	1.087, 1.088	1.052	1.069	1.156
7.55	0.25				2.091 to 2.199	1.154			
7.60	-0.25				2.079 to 2.160	1.195			
7.65	0.50					1.334			
7.70	-0.50					1.256			
7.75	0	1.157	1.072	1.084	2.334 to 2.416				
7.80	0.25								
7.85	-0.25				2.409	1.583			
7.90	0.50				2.521	1.927			
7.95	-0.50				2.486	1.397			
8.00	0	1.835	1.246	1.384	2.436 to 2.522	1.540 to 1.882	1.590 to 1.641	1.522 to 1.633	2.152 to 2.240
8.05	0.25	2.004							
8.10	-0.25	2.096			2.536 to 2.667	2.012			
8.15	0.50								
8.20	-0.50					2.203			
8.25	0	2.331	2.117	2.213		2.304			
8.30	0.25								
8.35	-0.25				2.625	2.429			
8.50	0	2.512	2.415		2.641 to 2.666	2.430 to 2.499	2.454	2.409	2.539
9.00	↓	2.684	2.616		2.722 to 2.735	2.637 to 2.668	2.632	2.594	2.679
9.25			2.682	2.706	2.738	2.667			
9.50		2.782	2.724		2.767 to 2.780	2.710 to 2.731	2.762	2.670	2.749
9.75		2.811	2.769	2.799	2.770, 2.776	2.745, 2.746			
10.00					2.777 to 2.790	2.772, 2.773	2.689 to 2.707	2.720	2.811
10.25		2.839		2.840	2.781 to 2.828	2.777 to 2.802			
10.50		2.847			2.815	2.807	2.773 to 2.797	2.749 to 2.767	2.824 to 2.843
10.75		2.825	2.825	2.843	2.827	2.812			
11.00		2.771	2.807		2.797 to 2.851	2.807 to 2.837	2.828	2.785	2.866
11.25		2.756	2.786	2.778	2.840, 2.844	2.823, 2.861			
11.50		2.764	2.743		2.832, 2.845	2.832			
11.75		2.798	2.758	2.760	2.825 to 2.853	2.827 to 2.843	2.829	2.776	2.837
12.00				2.834	2.859, 2.846	2.851			
12.25				3.306	2.886, 2.830	2.861			
12.50					2.812 to 2.863	2.830, 2.840	2.734 to 2.772	2.641 to 2.732	2.793 to 2.850
12.75					2.822 to 2.850	2.826			
13.00					2.809 to 2.842	2.769 to 2.798			
13.25					2.801, 2.809	2.791, 2.801	2.786	2.731	2.859
13.50					2.795 to 2.814	2.733 to 2.777			
13.75					2.770 to 2.806	2.776			
14.00	↓				2.767 to 2.796	2.720 to 2.768	3.316	3.448	3.101
8.00	-3.75								
↓	-2.75								
	-1.75								
	-0.75								
	1.25								
	2.25								
	3.25								
	4.25								
11.00	1.00	2.762			2.914, 2.881	2.857			
↓	2.00				2.932	2.873			
	3.00	2.960			3.022				
	4.00								
14.00	1.00				2.808 to 2.850				
↓	2.00				2.923 to 2.945	2.831			
	3.00				3.082	3.137			
	4.00								

TABLE II (Continued)

x, in.	z, in.	Run Number									
		27	28	29	30	31	32, 34, 36			33	37
		Static Pressure Ratio, p/p_∞									
7.00	0	1.061	1.064		1.052	1.045	1.043,	1.040,	1.055	1.028	1.105
7.25	↓	1.054	1.062	1.031	1.036	1.044	1.057,	1.029		1.048	1.107
7.50	↓	1.149	1.057	1.050	1.050	1.101	1.078,	1.042,	1.058	1.109	1.108
7.55	0.25	1.204	1.042	1.038	1.049	1.106	1.082,	1.032,	1.103	1.109	1.116
7.60	-0.25	1.247	1.074	1.051	1.046	1.166	1.265,	1.057,	1.123	1.440	1.145
7.65	0.50	1.600	1.044	1.048	1.045	1.258	1.156,	1.075,	1.090	1.237	1.251
7.70	-0.50	1.289	1.241	1.040							
7.75	0	1.507	1.167		1.049	1.493	1.639,	1.336,	1.390	1.762	1.439
7.80	0.25					1.731		1.598,	1.474	1.915	1.650
7.85	-0.25	1.692	1.513	1.091	1.077	1.921		1.770,	1.723	2.040	1.813
7.90	0.50	2.142	1.206	1.113	1.065	2.046		2.144,	1.690	2.142	2.064
7.95	-0.50	1.922	2.053		1.136	2.163	2.241,	1.686,	1.818	2.199	2.252
8.00	0	2.135	1.911		1.276	2.224	2.331,	2.142,	2.061	2.253	2.388
8.05	0.25						2.372,	2.440,	2.444	2.263	2.550
8.10	-0.25	2.288	2.185	1.284	1.576	2.351	2.441,	2.225,	2.268	2.329	2.613
8.15	0.50	2.408	2.041	1.325	1.689	2.426	2.448,	2.345,	2.341	2.315	2.739
8.20	-0.50	2.413	2.374	1.386	1.844	2.432	2.512,	2.359,	2.398	2.379	2.804
8.25	0	2.422	2.329	1.535	2.052	2.451	2.540,	2.451,	2.436	2.390	2.865
8.30	0.25										2.916
8.35	-0.25	2.485	2.421		2.220	2.513		2.512,	2.504	2.457	2.950
8.50	0	2.542	2.488	1.982	2.395	2.566		2.585,	2.587	2.497	3.068
9.00	↓	2.678	2.621	2.418	2.597	2.708		2.671,	2.684	2.596	3.183
9.25	↓	2.706	2.667		2.661	2.758	2.749,	2.687,	2.709	2.642	3.227
9.50	↓	2.740	2.710	2.579	2.711	2.775	2.772,	2.720,	2.783	2.669	3.271
9.75	↓	2.768	2.734	2.618	2.743	2.815	2.802,	2.747,	2.776	2.689	3.308
10.00	↓	2.784	2.762	2.644	2.774	2.816	2.823,	2.784		2.698	3.320
10.25	↓	2.803	2.770	2.657	2.782	2.835	2.843,	2.778,	2.797	2.713	3.329
10.50	↓	2.809	2.793	2.671	2.752	2.829	2.832,	2.778,	2.806	2.714	3.321
10.75	↓	2.825	2.815	2.675	2.716	2.810	2.829,	2.793,	2.778	2.693	3.298
11.00	↓	2.827	2.808		2.643	2.758	2.776,	2.756,	2.762	2.668	3.265
11.25	↓	2.834	2.797		2.584	2.762		2.743,	2.751	2.650	3.241
11.50	↓	2.824	2.794	2.624	2.566	2.738		2.724,	2.738	2.631	3.242
11.75	↓	2.807	2.764	2.562	2.677	2.771		2.736,	2.792	2.637	3.384
12.00	↓	2.767	2.719		3.141	3.010	2.896,	3.055,	3.072	2.876	3.918
12.25	↓	2.741	2.694	2.433	3.802	3.623					
12.50	↓	2.743	2.683	2.386							
12.75	↓	2.718	2.687	2.308							
13.00	↓	2.761	2.722	2.268							
13.25	↓	2.777	2.773	2.261							
13.50	↓	2.878	2.907	2.373							
13.75	↓	3.071	3.161								
14.00	↓										
8.00	-3.75				1.099	1.723		2.184,	1.784	2.050	
↓	-2.75				1.157	1.558		1.730,	1.594	2.042	
↓	-1.75	1.919	2.346		1.191	1.835		1.570,	1.752	2.145	
↓	-0.75	2.079	2.140		1.199	2.207		1.827,	1.948	2.279	2.406
↓	1.25	2.411	1.272			2.363		1.857,	1.802	2.144	
↓	2.25	2.448	1.506	1.100	1.225	2.329		1.981,	1.937	2.175	
↓	3.25				1.128	1.910		2.142,	2.132	2.243	
↓	4.25										
11.00	1.00	2.817	2.820	2.605	2.601	2.772		2.679,	2.717	2.575	3.241
↓	2.00	2.841	2.822	2.513	2.575	2.711		2.615,	2.692	2.587	3.205
↓	3.00				2.465	2.666		2.603,	2.734	2.655	3.217
↓	4.00				2.244	2.761			2.756	2.609	3.200
14.00	1.00										
↓	2.00										
↓	3.00										
↓	4.00										

TABLE II (Concluded)

x, in.	z, in.	Run Number						
		38	40	41	43	45	46	47
		Static Pressure Ratio, p/p_∞						
7.00	0	1.040	1.057	1.062	1.056	1.059	1.049	1.114
7.25	↓	1.053	1.062	1.095	1.054	1.064	1.167	1.111
7.50	↓	1.059	1.070	1.298	1.124	1.093	1.653	1.157
7.55	0.25	1.049	1.181	1.500	1.235			
7.60	-0.25	1.054	1.092	1.491	1.211			
7.65	0.50	1.071	1.316	1.880	1.547	1.336	1.786	1.615
7.70	-0.50							
7.75	0	1.214	1.378	2.035	1.750	1.747	1.938	1.878
7.80	0.25	1.356	1.685	2.221	1.920			
7.85	-0.25	1.346	1.595	2.206	1.953	2.096	2.011	2.416
7.90	0.50	1.703	2.078	2.369	2.217			
7.95	-0.50	1.510	1.761	2.231	2.158			
8.00	0	1.867	2.146	2.397	2.340	2.371	2.120	2.772
8.05	0.25	1.985	2.299	2.458	2.377			
8.10	-0.25	2.013	2.293	2.451	2.391			
8.15	0.50	2.118	2.441	2.533	2.468			
8.20	-0.50	2.103	2.342	2.471	2.432			
8.25	0	2.146	2.452	2.549	2.502	2.557	2.225	3.022
8.30	0.25	2.180	2.497	2.576	2.540			
8.35	-0.25	2.187	2.486	2.562	2.523			
8.50	0	2.241	2.562	2.615	2.578	2.638	2.284	3.131
9.00	↓	2.341	2.660	2.682	2.680	2.719	2.344	3.275
9.25	↓	2.351	2.677	2.725	2.690	2.758	2.364	3.314
9.50	↓	2.381	2.709	2.727	2.724	2.785	2.384	3.331
9.75	↓	2.400	2.733	2.759	2.743	2.817	2.410	3.372
10.00	↓	2.407	2.738	2.762	2.762	2.822	2.421	3.368
10.25	↓	2.413	2.761	2.775	2.774	2.827	2.418	3.358
10.50	↓	2.413	2.778	2.784	2.782	2.804	2.407	3.316
10.75	↓	2.392	2.786	2.788	2.790	2.785	2.373	3.246
11.00	↓	2.364	2.793	2.795	2.798	2.762	2.376	3.188
11.25	↓	2.352	2.799	2.790	2.808	2.774	2.373	3.202
11.50	↓	2.382	2.782	2.787	2.791	2.829	2.376	3.375
11.75	↓	2.454	2.759	2.772	2.778	3.036 to 3.057	2.438 to 2.470	3.920 to 3.989
12.00	↓	2.760	2.734	2.745		3.536 to 3.600	2.801 to 2.867	5.214 to 5.401
12.25	↓				2.744			
12.50	↓				2.730			
12.75	↓		2.747	2.861	2.721			
13.00	↓		2.791		2.727			
13.25	↓		2.873		2.738			
13.50	↓				2.820			
13.75	↓		3.545					
14.00	↓							
8.00	-3.75							
↓	-2.75							
↓	-1.75							
↓	-0.75	1.693						
↓	1.25							
↓	2.25							
↓	3.25							
↓	4.25							
11.00	1.00	2.382	2.817	2.802	2.831			
↓	2.00	2.404		2.822	2.837			
↓	3.00	2.384	2.823	2.809	2.821			
↓	4.00	2.386	2.820	2.820	2.828			
14.00	1.00							
↓	2.00							
↓	3.00							
↓	4.00							

TABLE III

TABULATED PRESSURE DATA FOR FACE AND TOP OF STEP, h = 0.96 IN.

$x-x_{step}$, in.	*z, in.	y, in.	Run Number							
			10	11	12	13	14	45	46	47
			Static Pressure Ratio, p/p_∞							
0	0.50	0.050				3.462	3.403	3.337 to 3.436	2.690 to 2.748	4.866 to 5.147
	0.75	0.100	3.401	3.424		3.537	3.482	3.284 to 3.396	2.660 to 2.699	4.567 to 4.655
	0.25	0.150	3.369	3.232		3.310	3.348	3.235	2.672	4.616
	0.50	0.200	3.186	3.059		3.185	3.271	3.149	2.603	4.300
	0.75	0.250	3.095	3.003		3.179	3.112	3.099	2.546	4.058
	0.25	0.300	3.044	2.967		3.027	2.968 to 3.118	3.115	2.670	3.924
	0.50	0.350				3.086	2.934 to 3.057	3.016	2.519	3.884
	0.75	0.400				3.023	2.983	3.011	2.704	3.789
	0.25	0.450				3.063	3.077	3.012	2.781	3.807
	0.50	0.500				3.110	3.031			
	0.75	0.550				3.272	2.975	3.325	2.924	4.170
	0.50	0.615				3.319	3.288	3.125	2.996	4.484
	0.25	0.660	3.499	3.625		3.466	3.776	3.186	3.075	5.040
	0.75	0.710	3.909	3.826		3.701	3.777	3.995	3.478	5.510
	0.50	0.760	4.165	4.536		4.038	3.936	3.839	3.571	6.419
	0.25	0.810	4.367	4.528		4.355	4.046	3.719	3.459	7.568
	0.75	0.860	4.731	4.765		4.867	4.101 to 4.519	4.778	3.953	
	0.50	0.910		5.922			4.014 to 4.604			
0.100	2.00	h	1.264		1.180	1.245		1.168	1.035	1.465
0.250			1.370		1.314	1.378	1.314	1.281	1.178	1.640
0.375						1.329	1.288			
0.500						1.280	1.259	1.251	1.182	1.590
0.625						1.276	1.247			
0.750			1.268			1.224	1.215 to 1.232			
1.000			1.205		1.224	1.190	1.199 to 1.207			
1.250			1.159			1.144	1.179			
1.500			1.127		1.167	1.122	1.147			
1.750			1.109		1.132	1.102	1.109	1.088	1.080	1.116
2.000			1.085		1.101	1.093	1.078			
2.250			1.066		1.071	1.084	1.092			
2.500			1.055		1.038	1.078	1.081			
2.750			1.034		1.033	1.076	1.062 to 1.075	1.083	1.096	1.175

For S and h values, see Table I.

*Tabulated values are for steps with a 9-in. span. For steps with S = 6 in., subtract 1.5 in. from the tabulated values in this column.

TABLE IV
TABULATED PRESSURE DATA FOR FACE AND TOP OF STEP, h > 0.96 IN.

x-x_{step}, in.	*z, in.	y, in.	Run Number (21) 15, 16	(20) 19	22	23	(Repeat of 22) 24
			Static Pressure Ratio, p/p_∞				
0	0.50	0.050	(3.919)	(4.049)			
	0.75	0.100	(3.688)	(4.092)			
	0.25	0.150	(3.921)	(3.820)			
	0.50	0.200	(3.788)	(3.722 to 3.857)			
	0.75	0.250	(3.623)	(3.720 to 3.851)			
	0.25	0.300	(3.772)	(3.573 to 3.624)			
	0.50	0.350	(3.541)	(3.569)			
	0.75	0.400	(3.407)	(3.624)			
	0.25	0.450	(3.479)	(3.335 to 3.408)			
	0.50	0.500	(3.316)	(3.338 to 3.398)			
	0.75	0.550	(3.222)	(3.419)			
	0.50	0.615	(3.413)	(3.349)			
	0.25	0.660	(3.361)	(3.258)			
	0.75	0.710	(3.318)	(3.432)			
	0.50	0.760	(3.408)	(3.280 to 3.356)			
	0.25	0.810	(3.511)	(3.361 to 3.410)			
	0.75	0.860	(3.470)	(3.509 to 3.630)			
	0.50	0.910	(3.266)	(3.172)			
	0.50	h-0.910	3.293, 3.311	3.669	3.179	3.251	3.195
	0.75	h-0.860	3.270, 3.589	3.764	3.124 to 3.171	3.299	3.100
	0.25	h-0.810	3.538, 3.593	3.849	3.121 to 3.174	3.258 to 3.543	3.248 to 3.301
	0.50	h-0.760	3.538, 3.551	3.670	3.180 to 3.257	3.202 to 3.618	3.201 to 3.260
	0.75	h-0.710	3.494, 3.495	4.002	3.174 to 3.236	3.241 to 3.392	3.157 to 3.301
	0.25	h-0.660	3.850, 3.912	4.264	3.218		3.399
	0.50	h-0.610	3.800, 3.830	4.415	3.354	3.495	3.389
	0.75	h-0.560	3.722, 3.721	4.514	3.359	3.574	3.373
	0.25	h-0.510	4.491	5.007	3.275 to 3.540	3.477 to 4.270	3.706 to 3.745
	0.50	h-0.460	4.277, 4.280	4.594	3.397	4.323	3.890
	0.75	h-0.410	4.089, 4.054	4.816	3.555	3.963	3.710
	0.50	h-0.345	4.758, 4.714	5.563	3.846	4.439	4.087
	0.25	h-0.300	5.452, 5.310	5.984	3.866 to 4.121	5.078	4.512
	0.75	h-0.250	4.778, 4.590	6.268	4.011 to 4.314	4.620 to 5.064	4.329 to 4.488
	0.50	h-0.200	5.357, 5.366	6.114	4.232 to 4.716	5.316 to 6.326	4.847 to 4.987
	0.25	h-0.150	6.559, 6.416	6.899	4.503 to 4.866	5.684 to 6.365	5.195 to 5.394
	0.75	h-0.100	5.179, 4.993	7.030	5.154	5.679 to 6.293	5.181
	0.50	h-0.050	5.618, 5.783	7.089	5.318	6.099	5.470
0.100	2.00	h	0.876, 0.863	0.981	1.105	1.113	0.976
0.250			1.160, 1.145	1.261	1.311 to 1.328	1.333	1.223
0.375			1.253, 1.244	1.331	1.316 to 1.348	1.313 to 1.347	1.240 to 1.254
0.500			1.254, 1.274	1.285	1.298 to 1.323	1.297 to 1.328	1.233 to 1.254
0.625			1.282, 1.302	1.304	1.266 to 1.300	1.270 to 1.306	1.242 to 1.256
0.750			1.302, 1.302	1.289	1.300	1.285 to 1.328	1.256
1.000			1.314, 1.317	1.243	1.278	1.276	1.253
1.250			1.292, 1.312	1.211	1.236	1.226	1.231
1.500			1.296, 1.307	1.152	1.156 to 1.179	1.155 to 1.188	1.191 to 1.206
1.750			1.299, 1.284	1.095	1.163	1.153	1.194
2.000			1.264, 1.268	1.044	1.112	1.084	1.148
2.250				1.001	1.058 to 1.083	1.008 to 1.030	1.131 to 1.137
2.500			1.263, 1.214	0.981	1.061 to 1.078	0.990 to 1.009	1.129 to 1.135
2.750			1.232, 1.232	0.943	1.072	0.970 to 0.986	1.128

For S and h values, see Table I.

*The tabulated values are for steps with a 9-in. span. For steps with S = 6 in., subtract 1.5 in. from the tabulated values in this column.

UNCLASSIFIED

Security Classification

DOCUMENT CONTROL DATA - R & D

(Security classification of title, body of abstract and indexing annotation must be entered when the overall report is classified)

1. ORIGINATING ACTIVITY *(Corporate author)*	2a. REPORT SECURITY CLASSIFICATION
Arnold Engineering Development Center ARO, Inc., Operating Contractor Arnold Air Force Station, Tennessee 37389	UNCLASSIFIED
	2b. GROUP N/A

3. REPORT TITLE

EXPERIMENTAL INVESTIGATION OF TURBULENT STEP-INDUCED BOUNDARY-LAYER SEPARATION AT MACH NUMBERS 2.5, 3, AND 4

4. DESCRIPTIVE NOTES *(Type of report and inclusive dates)*

Final Report April 29 to September 25, 1968

5. AUTHOR(S) *(First name, middle initial, last name)*

Jerry S. Hahn, ARO, Inc.

6. REPORT DATE	7a. TOTAL NO. OF PAGES	7b. NO. OF REFS
March 1969	38	3

8a. CONTRACT OR GRANT NO.	9a. ORIGINATOR'S REPORT NUMBER(S)
F40600-69-C-0001	
b. PROJECT NO. 8953	AEDC-TR-69-1
c. Task 03	9b. OTHER REPORT NO(S) *(Any other numbers that may be assigned this report)*
d. Program Element 62201F	N/A

10. DISTRIBUTION STATEMENT

This document has been approved for public release and sale; its distribution is unlimited.

11. SUPPLEMENTARY NOTES	12. SPONSORING MILITARY ACTIVITY
Available in DDC.	Arnold Engineering Development Center (AELR), Arnold Air Force Station, Tennessee 37389

13. ABSTRACT

An experimental investigation of turbulent separated boundary-layer flow was conducted using high ($3 \lessapprox h/\delta \lessapprox 13$) forward-facing steps (with side plates) mounted on a flat plate at zero angle of attack. The tests were made at Mach numbers of 2.5, 3.0, and 4.0 for Reynolds numbers, based on the boundary-layer total thickness at the separation location, from 0.10×10^6 to 0.15×10^6. The effects of Mach number, step height and span, end plates, and step-face fairings were investigated. Data are presented graphically and in tabulations and include model surface pressures on the flat plate and on the face and top of selected steps, boundary-layer Mach number profiles, and selected oil dot photographs.

DD FORM 1 NOV 65 1473

UNCLASSIFIED

Security Classification

14. KEY WORDS	LINK A		LINK B		LINK C	
	ROLE	WT	ROLE	WT	ROLE	WT
boundary layer separation						
flat plate models						
wind tunnels						
supersonic flow						

AFSC
Arnold AFS Tenn